Summary of Studies of SiD ECal Manual Calibration

Amanda Steinhebel, James Brau
University of Oregon, Center for High Energy Physics,
1274 University of Oregon Eugene, Oregon 97403-1274 USA
(Dated: March 8, 2018)

SiD is one validated detector design for the International Linear Collider with strength in particle flow calorimetery. The silicon-tungsten electromagnetic calorimeter greatly contributes to this. Layers of highly granular (13 mm^2 pixels) silicon detectors embedded in thin gaps ($\sim$1 mm) between DENS-24 tungsten alloy plates give the SiD ECal energy resolution on the scale of $20\%/\sqrt{E}$. For use within the full SiD simulation, a robust, nonlinear calibration technique is developed that considers the effect of leakage. This calibration achieves good precision for a wide range of true particle energies all with the calibration error per energy resolution remaining below 3%.

I. SID CALORIMETER BACKGROUND

In the SiD design, the electromagnetic calorimeter (ECal) barrel sits between the silicon tracker and hadron calorimeter (HCal) at an inner radius of 1.264 m from the interaction point with a z extent of 3.53 m. It is made of twelve trapezoidal modules that extend the full z length of the detector with overlapping ends to avoid projective cracks through the detector. This creates a structure that is periodic in increments of $\pi/6$ radians (Fig. 1 shows the view from the xy plane with the z dimension coming out of the page, and indicates the angle φ). Each module consists of 31 layers of pixelated silicon wafers and 30 layers of DENS-24 tungsten alloy. The first layer of each module is a silicon tracking layer, followed by twenty iterations of 2.5 mm DENS-24 and a 1.25 mm gap in which the 0.3 mm silicon layer resides (Fig. 2). This is followed by ten iterations of 5 mm DENS-24 and the same 1.25 mm silicon-containing gap. Therefore, the ECal begins and ends with a sensitive silicon layer. This structure is identically repeated for all twelve modules. The regions of module overlap comprise approximately 30% of the detector. Showers that develop in these regions deposit charge into both modules, though layers of the two modules are at an angle relative to each other. A smaller subset of the overlap region contains only thin layers of tungsten absorber, and none of the thicker 5 mm tungsten layers. This geometry has important physical effects on the detector[1], such as tungsten depth varying as a function of φ.

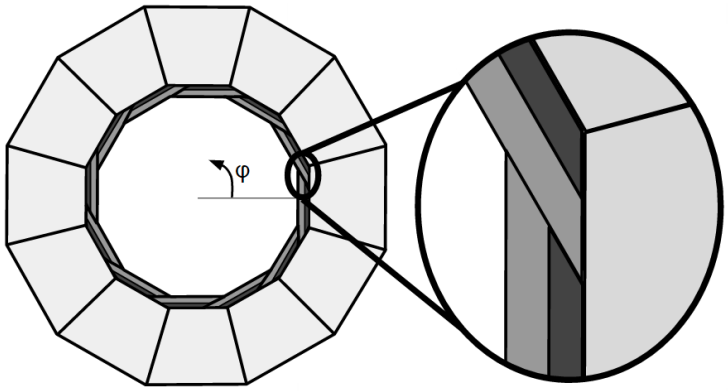

FIG. 1: The SiD ECal (darker shades) is surrounded by the HCal (lighter shade) and made of twelve overlapping trapezoidal modules to avoid projective cracks. The cutout image illustrates the overlap region of these ECal modules, where the darkest shade indicates areas with thick tungsten layers and the medium-colored shade indicates areas with thin tungsten layers. The image shows the view from the xy plane with the z dimension coming out of the page, and indicates the angle φ.

[1] A more extensive review of the ECal geometry and its impact on physics can be found in the note "SiD ECal Geometry" (`http://pages.uoregon.edu/asteinhe/SiDNotes/geometry/`).

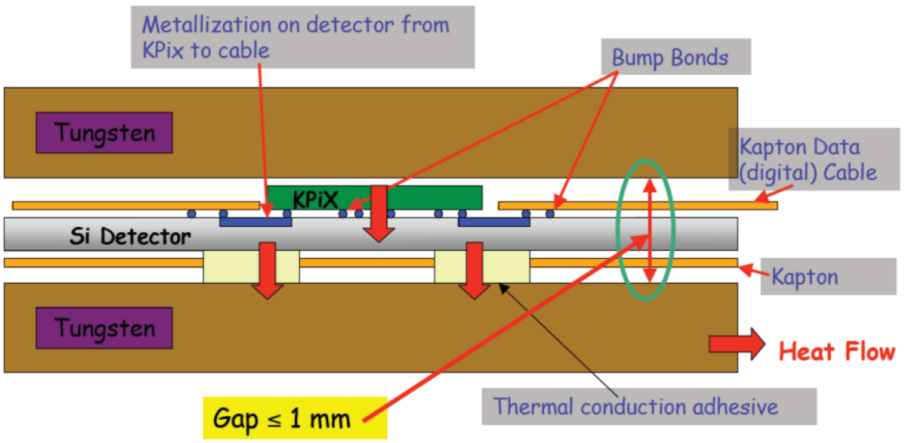

FIG. 2: The 1.25 mm gap between tungsten absorber layers includes a 0.3 mm silicon sensor layer bump-bonded to the KPiX readout chip. [Figure credit: Martin Breidenbach, SLAC]

Similarly, the SiD HCal is designed with twelve identical trapezoidal modules that pair one-to-one to ECal modules. The HCal design involves no overlap feature (see Fig. 1) but instead contains projective cracks out from the interaction point. The HCal is a scintillating sampling calorimeter with forty pairs of 3 mm thick polystyrene scintillator and 19 cm thick stainless steel absorber layers. The high granularity of both of these calorimeters is crucial to execute SiD's particle-flow strategy.

All the following studies were conducted using the full SiD simulation, `SiD_o2_v02`. Samples of five thousand single photons are directed into the full detector simulation at normal incidence to the ECal surface ($\theta = 90^o$, $\varphi = 0^o$). Studies were performed with a range of photon energies, including $1, 2, 5, 10, 20, 50$, and 100 GeV. Only depositions in the calorimeter barrels (not endcaps) are considered.

All figures shown here and raw data files can be found at `http://pages.uoregon.edu/asteinhe/SiDNotes/calibrationLeakageStudies/` and the analysis scripts used to generate them can be found at `http://github.com/SiliconDetector/UserAnalyses/tree/master/asteinhebel_ECalAnalysis/calibrationLeakageStudies`.

II. CALIBRATION MOTIVATION

The main goal of this project is to determine ECal calibration constants from first principles - that is, to understand the physical motivations behind each element of calibration. Detector properties such as geometry play a role, as well as the nature of the calorimeter. The SiD ECal is a solid state sampling calorimeter, so due to the presence of the passive tungsten layers the majority of each electromagnetic shower is lost to the tungsten and not read out by the electronics that interface with only silicon layers. In general, less than 1.75% of a photon's true energy is measured from deposits from the ECal. In order to recover this information and properly reconstruct properties of the particles using only the available information in the silicon layers, calibration is essential.

Due to the ECal's high granularity and sensitivity, high energy resolution[2] is achieved. For the full range of investigated true energies, the scaled energy resolution of only ECal deposits is shown in Fig. 3. In general, this value falls around the expected 20% [3], however higher energies trend higher indicating a wider spread of the distribution of energies. This effect is thought to be caused by leakage of shower energy out of the ECal and into the HCal that follows. This idea is explored in more detail in Section IV.

[2] Here, energy resolution is defined as the standard deviation of the measured energy distribution divided by its mean (Energy resolution is defined as σ/μ from Gaussian fits. Deposits in silicon layers following 5 mm thick tungsten are weighted by 2 to account for the sampling fraction.). In general, this is proportional to some percentage around $20\%/\sqrt{E}$. The scaled energy resolution is the energy resolution multiplied by $\sqrt{E}$ which shows the $\sim 20\%$ value.

[3] This value differs from the TDR reported value of $17\%/\sqrt{E}$ [1]. This could be due to a number of factors, including: the current state of the SiD simulation, simulated ECal granularity, particle shower types utilized, distribution of showers within the detector, and energy of showers. As the SiD simulation and collaboration continues to progress, this discrepancy should be revisited.

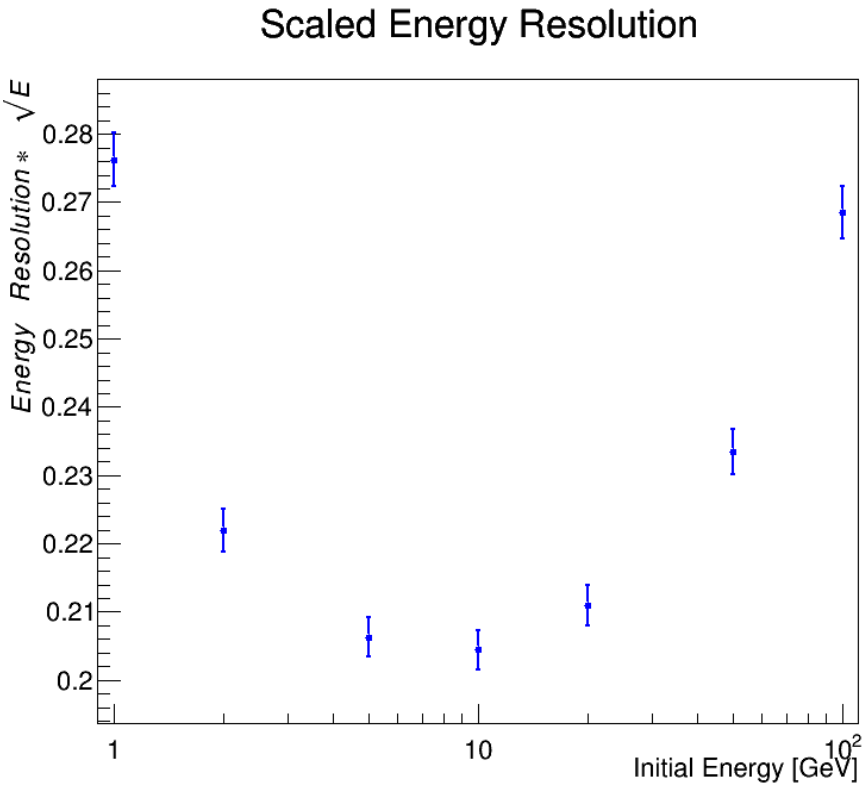

FIG. 3: The scaled energy resolution ($\sigma/\mu * \sqrt{E}$) of the SiD ECal for 5000 photon events at each energy. These values generally fall around 20% as expected, but increase at higher energies due to leakage of shower energy out of the ECal and into the HCal.

Calibration of the ECal is investigated using only electromagnetic showers from incident photons and deposits in the ECal only. Studies involving the calibration of the HCal are in progress at the University of Texas Arlington.

III. LINEAR CALIBRATION

Historically, SiD has relied upon a linear-fit model for calorimeter calibration. In this way, one calibration constant is introduced for each calorimeter to effectively shift the measured distributions to values that more accurately reflect the true properties of the particle shower. A simple calibration is defined by Eqn. 1 with calibration constants a and z,

$$E_{calibrated} = aE_{measured,ECal} + zE_{measured,HCal} \ . \tag{1}$$

In this case of ECal calibration, $z = 0$ and only one calibration constant associated with the ECal measured energy remains:

$$E_{calibrated} = aE_{measured,ECal} \ . \tag{2}$$

This constant is optimized by plotting expected reconstructed energy and calculated calibrated energy and fitting the resulting plot with a linear fit. The more accurate the calibration, the closer the best fit line approaches $y = x$.

A toy calibration model was designed in Julia and distributed by Jan Strube [2]. This calibration method sums the contributions of all measured ECal hits for each event with a factor of two correction for the sampling fraction change in the back thicker tungsten layers. Only deposits in a cone of 0.2 radians from the true particle trajectory

are accepted and those outside the cone are rejected as backscatter or shower spreading[4]. These collections of event deposits for each true energy are then input to a line-fitting method with a preset calibration equation (such as Eqn. 2) and seeded calibration constant value. The ratio of the mean of the calibrated distribution to the true shower true energy is computed. This process iterates, altering the calibration constant until the ratio value is optimized and a final calibration constant is extracted. This is done simultaneously for showers of all energies, so one single calibration constant is used for all showers regardless of true energy.

For the SiD ECal, this linear, iterative process gives a calibration constant around $a \sim 58$. For a value of $a = 58.464$,[5] the mean of the calibrated energy distribution vs the true energy is shown in Fig. 4 with a linear best fit line of $y = 0.06 + 0.99x$, where y is the linearly calibrated energy and x is the true energy.

Similarly, the ratio between the calibrated distribution mean and the expected energy value should approach unity for each point. This is shown in Fig. 5 for energy deposits contained within the ECal. Instead, it is seen that higher energy showers experience worse calibration than lower energy showers. The ratio decreases at high energy, indicating that the calibration constant is too small. This is thought to be due to shower leakage, or the deposition of shower energy in the HCal. When particles interact with the ECal at high energy, the shower development is delayed and begins deeper in the calorimeter. This allows for normal shower development to occur through both the ECal and HCal. This can be seen in Fig. 6 where deposits in lower energy shower (10 GeV in (a)) are fully contained within the ECal (shown in Fig. 6 (a) ii, where the outer container is the ECal) but deposits in high energy showers (100 GeV in (b)) continue into the HCal (outside of the ECal container in Fig. 6 (b) ii). Since only ECal deposits are being considered, the portion of the shower deposited in the HCal is completely neglected here. If those deposits were known and added back into the original measured shower energy, the calibration would be more successful at high energy.

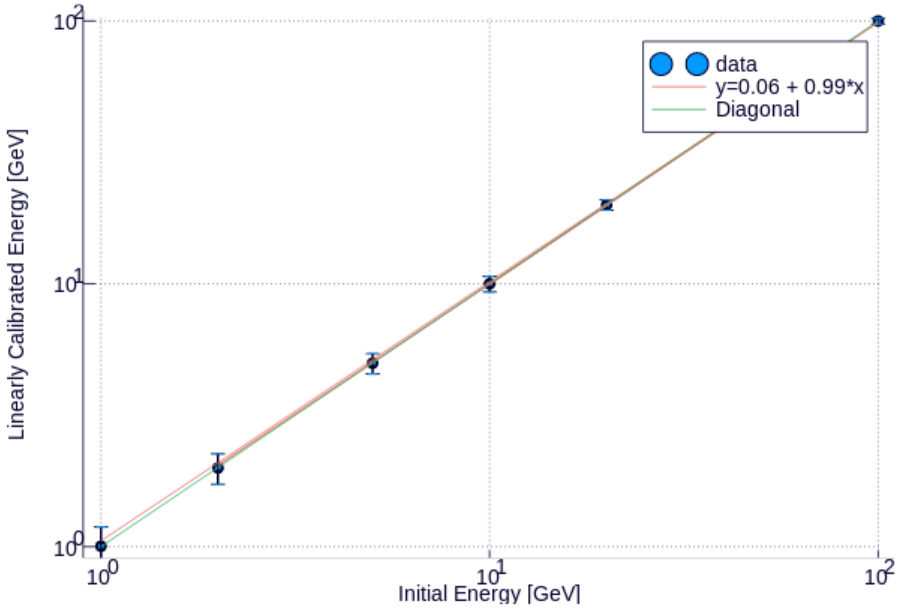

FIG. 4: The best linear fit when comparing the expected, true shower energy with the linearly calibrated, reconstructed energy where the calibration constant $a = 58.464$. The best fit line of $y = 0.99x + 0.06$ approaches the ideal case of $y = x$.

[4] A more extensive review of backscatter/shower spreading in the SiD ECal can be found in the note "SiD ECal Shower Spreading and Backscatter Studies" (`http://pages.uoregon.edu/asteinhe/SiDNotes/backscatter/`).

[5] This value is the linear coefficient of a non-linear calibration technique, approximating a pure linear coefficient. For more details on how this number was chosen, see Section V.

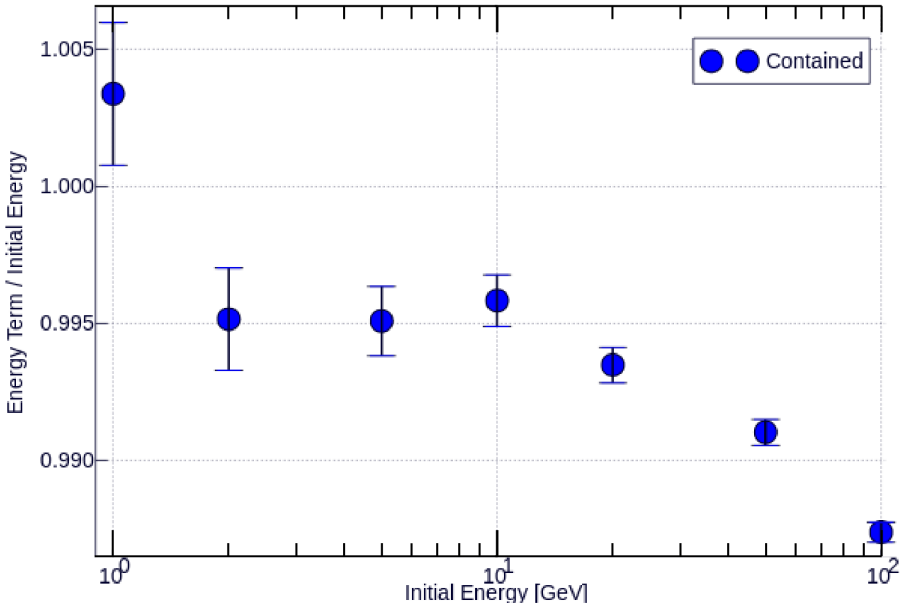

FIG. 5: The ratio of mean linearly calibrated energy ($a = 58.464$) to its expected value for deposits contained within the ECal. For perfect calibration, this value should approach unity for every true energy. The decrease in this value at high energies is an indication of shower leakage.

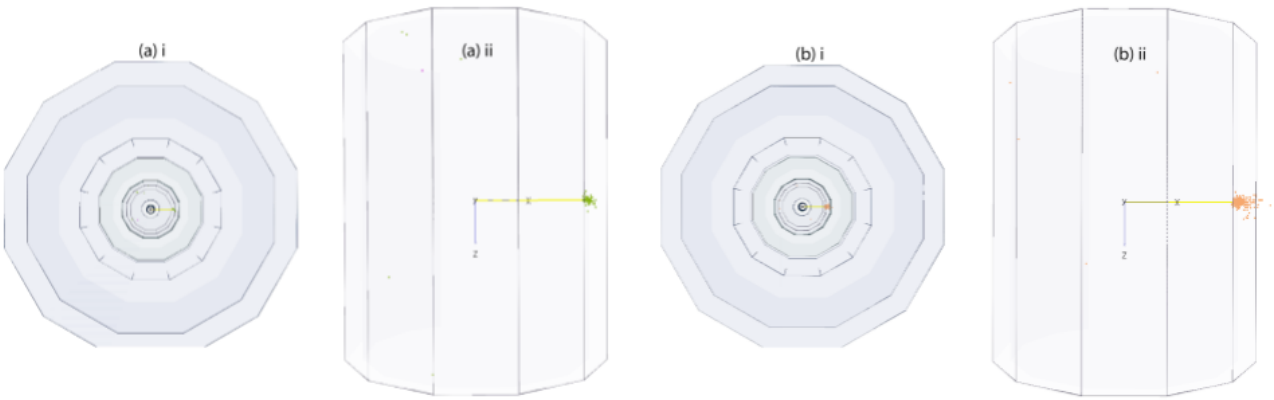

FIG. 6: Event displays for photons showers of (a) 10 GeV and (b) 100 GeV. The first set of images (i) show the entire SiD detector from down the beamline. The original photon path is shown in yellow and calorimeter deposits are shown in green or orange. The second set of images (ii) show only the ECal (from the xz plane) along with the photon path and calorimeter deposits. The lower energy shower (a) is fully contained within the ECal whereas the high energy shower (b) has deposits that leak into the HCal. This leakage leads to poor linear calibration at high energy.

IV. LEAKAGE ESTIMATION

In order to consider the effects of leakage on ECal calibration while continuing to exclusively use ECal barrel deposits (in order to preserve ECal energy resolution), multiple methods of leakage estimation were designed and tested.

A simple way of estimating leakage is to consider the uncalibrated HCal deposits associated with each electromagnetic shower event. Though straightforward, this method is less than optimal due to uncertainty in HCal calibration. Additionally, the leakage is estimated to be around 1% of the total measured shower energy for 100 GeV photon showers (the highest incident energy considered and therefore the largest leakage effect). Therefore, this small effect is difficult to reconcile with already sparse HCal deposits and the original intention to consider only ECal deposits.

Another straightforward approximation is to consider the back few ECal layers in order to estimate HCal deposits. The energy deposited in the final two ECal layers is shown in Fig. 7 for 1, 10, and 100 GeV photon shower. Showers largely contained within the ECal (see. Fig. 6) see few deposits in these back layers whereas high energy showers that leak into the HCal have more substantial depositions in these back layers - averaging 0.003% of the total shower energy for 100 GeV photons.

It should be restated that the entirety of the analysis presented in this note were conducted with showers at normal incidence to the ECal ($\theta = \varphi = 0^o$). Due to the geometry of the ECal, the total tungsten absorber depth varies as a function of φ and reaches a minimum where ECal modules overlap, leading to leakage that is not only energy- but also angle-dependent. This is shown in Fig. 8 where the percentage of 10 and 100 GeV photon showers deposited in the HCal increases to a maximum amount in areas where ECal modules overlap. In order to completely consider leakage effects in calibration, this angular effect must also be considered. This has not yet been rigorously investigated.

To most thoroughly estimate leakage with only ECal deposit information, the ECal shower profile is extrapolated into the HCal region. This allows for the well-established shower shape to dictate estimated leakage. Two different extrapolation techniques were considered, each considering different regions of the ECal.

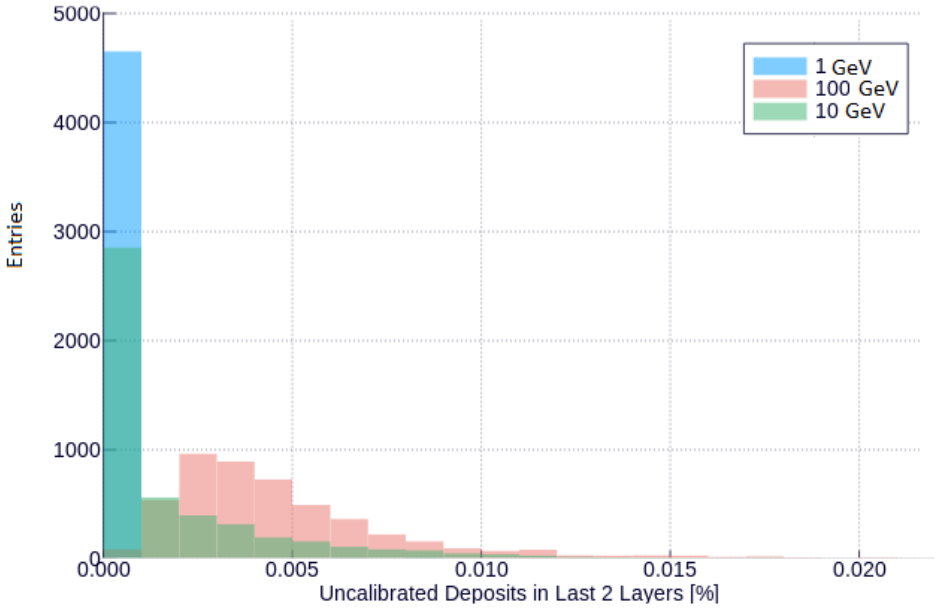

FIG. 7: Percentage of photon shower energy that is deposited in the last two layers of the ECal. 1 GeV showers, shown in blue, are fully contained within the ECal and rarely have deposits near the back of the calorimeter. Higher energy showers such as at 10 GeV shown in green see slightly more deposits, indicating incomplete containment. The highest energy showers at 100 GeV (in pink) have the largest amount of leakage and also measured deposits in the back of the ECal, with deposits in the final two layers containing roughly 0.003% of the total shower energy.

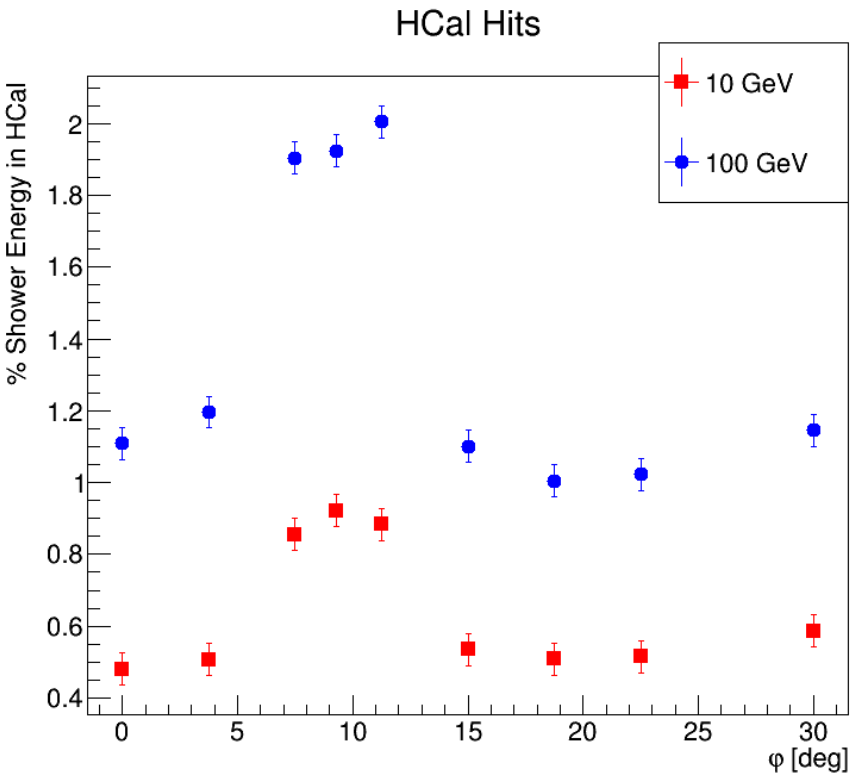

FIG. 8: Percentage of photon shower energy that is deposited in the HCal, indicating shower leakage. Higher energy showers (100 GeV, shown with blue circles) generally produce more leakage than lower energy showers (10 GeV, shown with red squares). The leakage also varies as a function of φ, with the most leakage in areas where ECal modules overlap due to less total tungsten absorber in those regions.

A. Linear Shower Extrapolation

ECal shower profiles are created by summing all measured deposits in each ECal layer individually. For each true photon energy, the mean of the collection of each layer energy is recorded and plotted as a function of length into the calorimeter. This is determined by the calculated location of that layer at normal incidence. Standard simulation units use [GeV] for measured energy deposits and [mm] for depth into the calorimeter (where the ECal spans from $1264 - 1403$ mm radially from the interaction point). The measured energy in some calorimeter range can then be found by calculating the integral under the curve. Leakage is defined as the scaled integral of the curve within the HCal region.

To gauge the accuracy of the extrapolation methods in estimating leakage, the shower profile is extended to include the average deposits in all ECal and HCal deposits. In order to eliminate unit-dependent effects due to different material properties of the two calorimeters, energy units of number of minimum ionizing particles (MIPs) are instead used. In silicon, 1 MIP ≈ 0.124 MeV while in scintillating polystyrene 1 MIP ≈ 0.604 MeV. Rather than measuring the distance from the interaction point in millimeters, lengths are recorded with the number of radiation lengths $[X_0]$ of absorber ($1\ X_0 \approx 3.85$ mm for the tungsten alloy of the ECal, and $1\ X_0 \approx 17.6$ mm for the stainless steel of the HCal) before each active layer. This corrects for any sampling fraction effects.

The first extrapolation method exploits the approximately exponential nature of the tail of the electromagnetic shower. On a semi-log plot (with the y axis utilizing a log scale), this exponential nature looks linear where

$$y_{fit} = e^{b+mx} \ .$$

The final five ECal layers are fit with a linear function, which is extrapolated into the HCal region. This should approximate the continued development of the shower into the HCal region. With this method, a scaled radiation length unit is used. The ECal portion contains standard radiation lengths, but the HCal radiation lengths are scaled

like

$$X_0 \cdot \left(\frac{(dE/dx)_W}{(dE/dx)_{SS}} \right) = X_0 \cdot \left(\frac{20.2665}{12.1338} \right) \approx 1.67 \ X_0 \ ,$$

where the subscripts denote absorber material (tungsten alloy or stainless steel).

Figure 9 shows the shower development curves in the ECal and HCal for (a) 1 GeV, (b) 10 GeV, and (c) 100 GeV photon showers, where each black star indicates an active calorimeter layer. The black vertical line near $X_0 = 26$ indicates the transition from ECal layers to HCal layers. The red line is the linear best fit curve fit to the final five ECal layers and extrapolated into the HCal region. With the scaled radiation length units, the shower development curve is smooth and the fit extrapolation closely matches the true HCal behavior. Constants associated with each fit are given in the plots. It can be seen that as the true particle energy increases, the slope of the linear fit trends toward zero. This implies that that there is a larger area contained under the fit and therefore more leakage.

With the best fit line extrapolated into the HCal region, the percent leakage $\mathcal{L}$ can then be estimated by integrating under the HCal portion of the curve and correcting units -

$$\mathcal{L} = \frac{\mathcal{I} \ [\text{MIPs} \cdot X_0]}{E_{measured,ECal}[\text{MIPs}] \cdot 1.3[X_0]} \ , \tag{3}$$

where $\mathcal{I}$ is the value of the integral under the linear fit from $26 < X_0 \lesssim 115$, or where $y \to 10^{-10}$. The value of $1.3 \ X_0$ in the denominator reflects the length in radiation length of one thick tungsten layer (or 5 mm $\cdot$ 0.26 X_0/mm). Scaling the HCal radiation length while leaving the ECal radiation lengths unaltered means that the integral formula of Eqn. 3 can be used when plotting both in radiation lengths and also scaled radiation lengths. The results of these integral calculations are shown in Subsection IV B, Fig. 11.

B. Gamma Distribution Extrapolation

The extrapolation of shower shapes can be made more precise by taking advantage of the information contained in the entire shower, rather than extrapolating based upon the large-X_0 limit of the exponential tail. The overall shower follows a gamma distribution with a tail that can be approximated as an exponential (as exploited above in Subsection IV A) [3], [4].

Identical shower development curves are created for this leakage estimation method, this time using standard units of radiation lengths (rather than scaled radiation lengths). The entire ECal distribution is then fit to a gamma function, where

$$y_{fit} = Ax^{\alpha}e^{-bx} \ .$$

Curves fit with this function are shown in Fig. 10 for (a) 1 GeV, (b) 10 GeV, and (c) 100 GeV photon showers. Again, the vertical line indicates the transition from ECal to HCal region and the red line is the gamma distribution fit to the ECal and extrapolated into the HCal region.

With these units, a characteristic tail of simulated energy deposits at large radiation length values (deep in the HCal) is noted. It is believed that this is an artifact of the simulation rather than a physical effect, as the tail plateaus with a nonphysical value of around 0.01 MIP. This could be caused by a MIP cut imposed earlier in the simulation process. Therefore, these plots should be physically considered at values of 1 MIP and larger.

The leakage percentage can be estimated identically to before with Eqn. 3. Figure 11 show the percentage integral value of both the linear fit of Subsection IV A and the gamma distribution fit of Subsection IV B compared to the percent of the uncalibrated shower energy contained in the HCal obtained through direct measurement. All three leakage estimation methods follow similar overall trends as a function of true particle energy, further indicating that they are all appropriate leakage estimation techniques. All three curves seem to follow a $\sqrt{x}$ shape, where x (as on the plot) is the true particle energy.

C. Event-By-Event Leakage Correction

The leakage estimation methods described in Subsections IV A and IV B estimate leakage generally for some defined energy, simulated five thousand times. In that way, the leakage estimation is based on average shower shape. In reality, each photon shower will include fluctuations making it distinct from other showers even within the same distribution.

An identical leakage estimation method can be used to estimate the leakage of every individual event, rather than just for the full distribution, by plotting each event's shower development curve and individually fitting a gamma

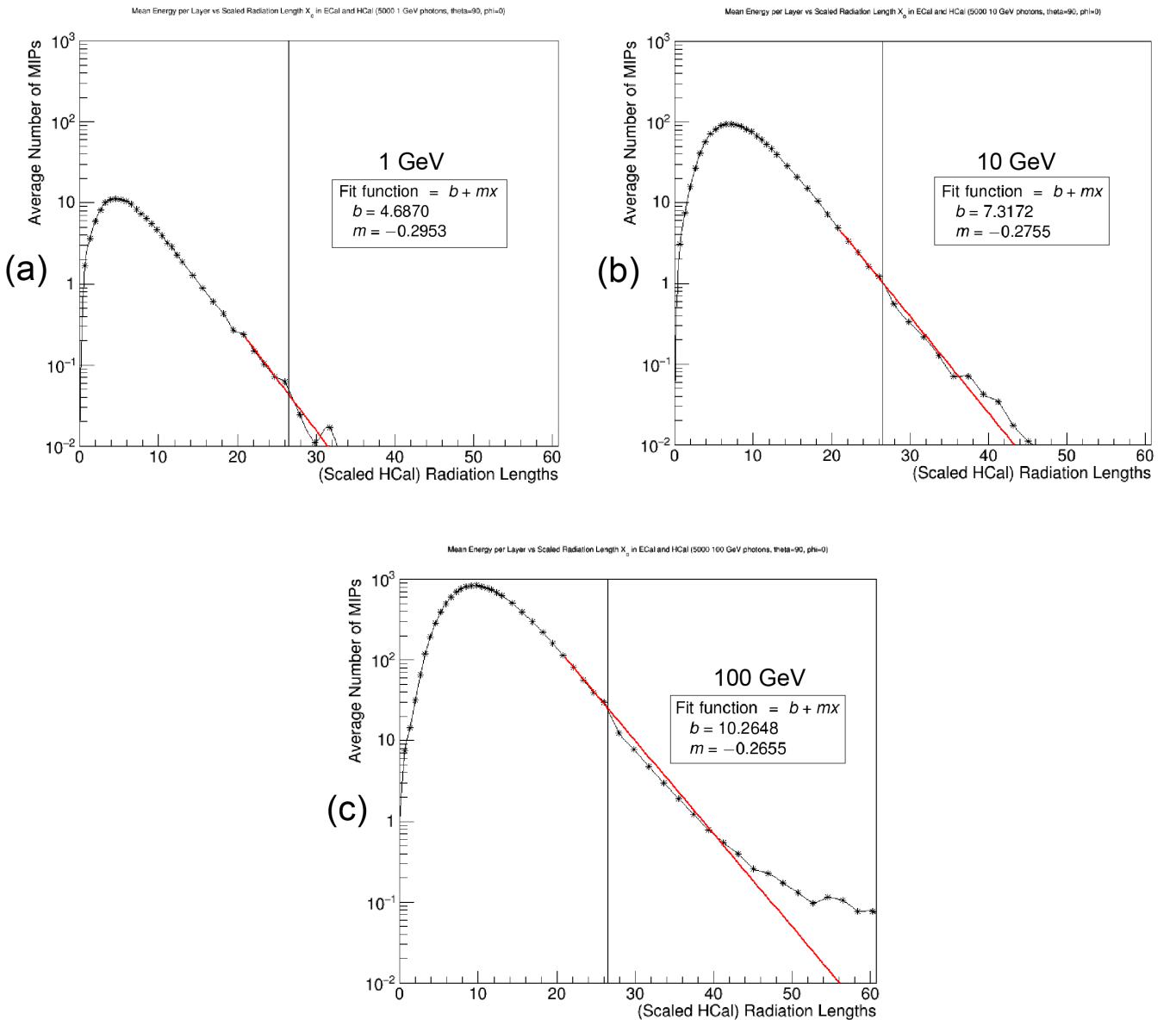

FIG. 9: Shower development curves through ECal and HCal active layers with a linear fit made to the final five ECal layers and extrapolated into the HCal region for (a) 1GeV, (b) 10 GeV, and (c) 100 GeV photon showers. The vertical line indicates the transition from ECal to HCal. The legends indicate fit parameters and show that as shower energy increases, the fit slope decreases leading to a larger integral value and therefore larger leakage. The integral under the HCal region of the linear extrapolation is an estimate of leakage.

distribution to each. This event-by-event leakage estimation allows for a more precise leakage correction that can take individual event fluctuations into account. Figure 12 shows four showers from 100 GeV photons and their associated gamma distribution fits, showing that even with event-dependent fluctuations the fit is robust enough to estimate event leakage percent. Showers from lower energy particles tend to have larger fluctuations and overall worse fits. Of the five thousand showers from 1 GeV photons, roughly 10% of events could not be successfully fit whereas only 1% of showers from 100 GeV photons had divergent fits.

The energy contained within the leakage of each event, $\mathcal{L}[MIP \cdot X_0]/1.3[X_0]$, is then added back into the energy

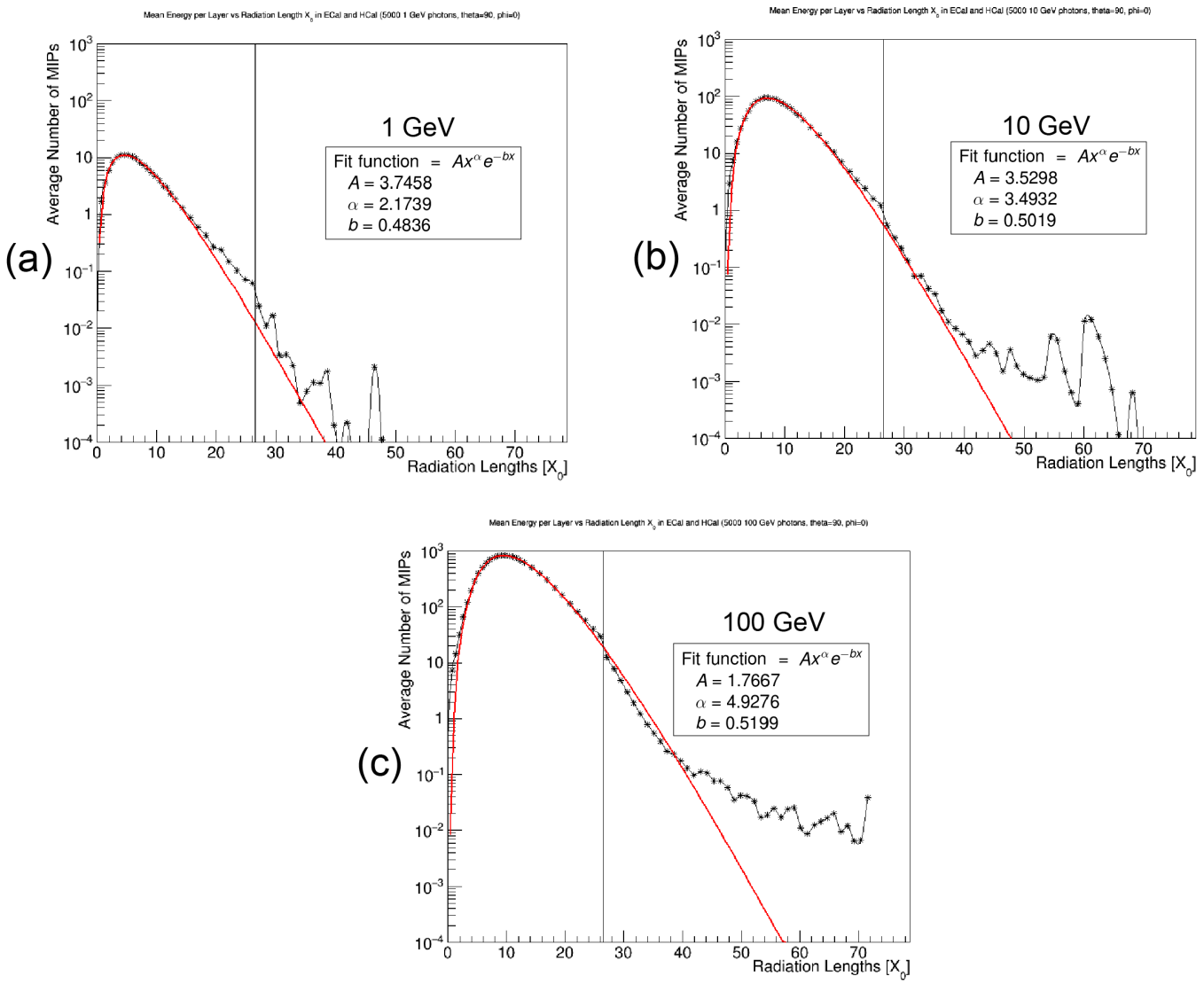

FIG. 10: Shower development curves through ECal and HCal active layers with a gamma distribution fit made to the all ECal layers and extrapolated into the HCal region for (a) 1GeV, (b) 10 GeV, and (c) 100 GeV photon showers. The vertical line indicates the transition from ECal to HCal. The legends indicate fit parameters. These plots should largely be considered for MIP values of unity or larger, as deposits with fractions of a MIP are likely nonphysical simulation effects.

measured for each event[6]. This is then used to create a new bulk distribution for each true particle energy, and the overall energy resolution can be recalculated. Figure 13 shows this new scaled energy resolution including event-by-event leakage correction (in red) compared to the uncalibrated scaled energy resolution (shown in blue and identical to Fig. 3). This leakage correction does not impact showers from low energy photons because the leakage added back into the event is so small. At high energies, especially 100 GeV, the event-by-event leakage correction significantly reduces the scaled energy resolution by sharpening the distribution. Incorporating event-by-event leakage correction leads to a 2.7% reduction in scaled energy resolution for showers from 100 GeV photons and leaves other showers from lower energy photons unaffected. This method is one way to begin accounting for HCal leakage in ECal calibration, and regain high energy resolution even with electromagnetic showers from high energy particles.

[6] Events that cannot successfully be fit have no leakage-related energy added back into the total event energy.

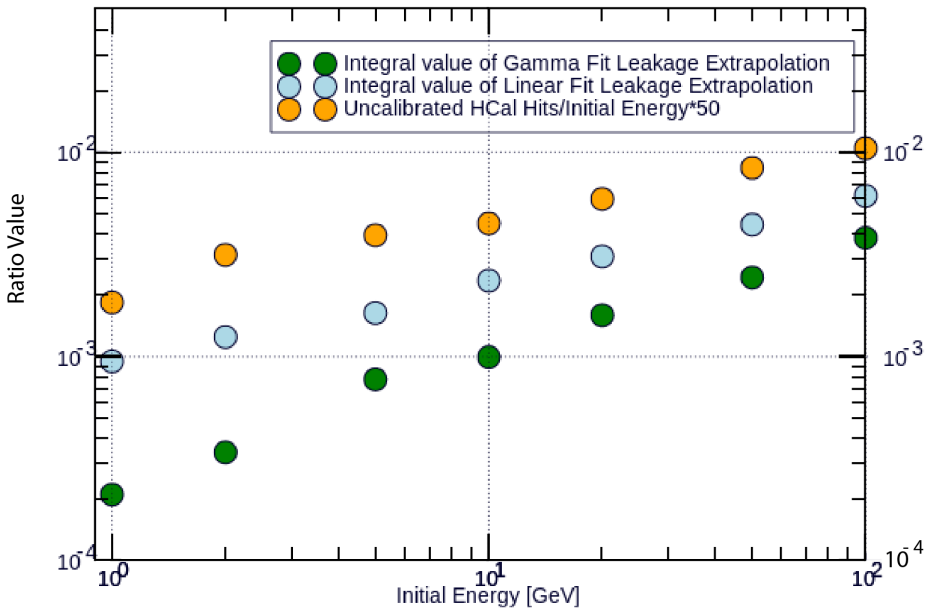

FIG. 11: The percentage integral values of both linear and gamma distribution fits follow a similar trend as uncalibrated HCal deposits. This indicates that the leakage estimation techniques involving shower development fitting are both appropriate estimators of leakage.

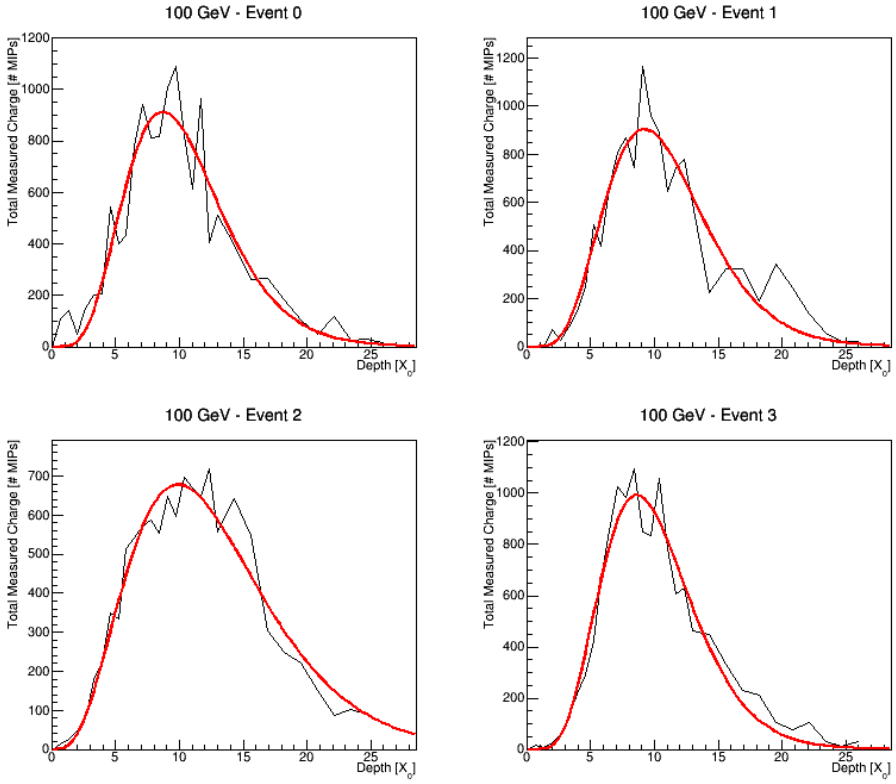

FIG. 12: The first four 100 GeV shower distribution curves, each individually fit by gamma distributions. These were used to estimate leakage on an event-by-event basis, and add that missing energy back into the overall 100 GeV photon distribution.

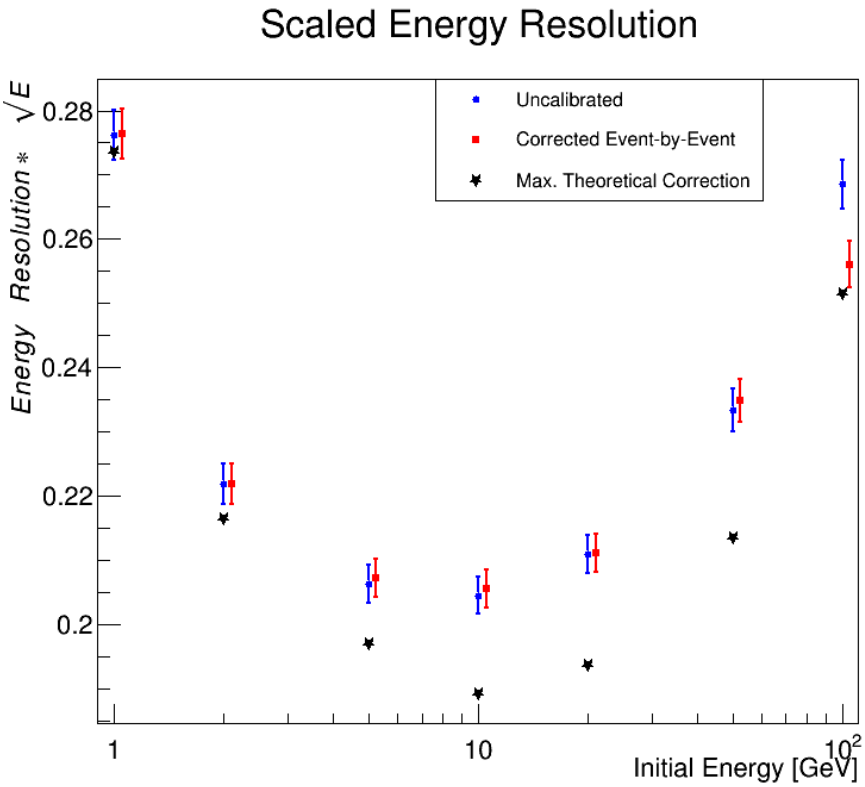

FIG. 13: The scaled energy resolution ($\sigma/\mu * \sqrt{E}$) of the SiD ECal for 5000 photon events at each energy. Blue circles indicate values from uncalibrated showers, whereas red squares incorporate estimated leakage on an event-by-event basis. Including this leakage leaves showers from low energy photons unaffected while showers from high energy photons with large leakage (especially 100 GeV) see a 2.7% decrease in the scaled energy resolution.

V. NON-LINEAR CALIBRATION

Section III showed that decent ECal calibration is possible using one overall calibration coefficient found from optimizing a linear fit method. However, leakage also plays a role in ECal calibration especially at high energies. One way to account for this leakage within the calibration without incorporating HCal information can be done by altering the calibration equation, Eqn. 2, to include a term that compensates for expected leakage. This still must be done delicately in order to not pollute the energy resolution.

Since leakage is energy dependent, we assume an additional term in Eqn. 2 to compensate for leakage where the leakage term is dependent upon the energy measured in the ECal to some power $(n+1)$. This term then also has its own calibration constant b, where

$$E_{calibrated} = aE_{measured,ECal} + bE^{n+1}_{measured,ECal} = E_{measured,ECal}\left(a + bE^{n}_{measured,ECal}\right) \ .$$

The exponent n can then be deduced from the nature of the estimated leakage. The nonlinear nature of this leakage term leads to an overall nonlinear calibration of the ECal.

From Section IV and Fig. 11, the power n can be identified as $n = 1/2$. That makes a final calibration equation of

$$E_{calibrated} = E_{measured,ECal}\left(a + bE^{1/2}_{measured,ECal}\right) \ . \tag{4}$$

With this simple change, the Julia toy calibration code introduced in Section III can be used identically to optimize an overall linear fit for two calibration constants, a and b. Again, these two constants are universal for photons of any true energy. The full process yields

$$\begin{aligned} a &= 58.464 \pm 0.2037 \\ b &= 0.5941 \pm 0.30327 \ . \end{aligned} \tag{5}$$

The accuracy of this full, nonlinear calibration procedure can be directly compared to the approximate linear procedure (using the linear coefficient a) from Section III. The correlation between calibrated energy and true energy of Fig. 4 can be directly compared to Fig. 14 where the nonlinear fit performs better with a best fit line of $y = 1.00x - 0.01$.

The small nonlinear term, as expected, has a much smaller effect on the overall calibration than the dominant linear term. This is shown in Fig. 15 where the linear and nonlinear energy contributions are shown as a ratio between each term and the expected, true energy (for example, the yellow linear calibration terms are showing $aE_{measured,ECal}/E_{true}$). Though the contribution of the nonlinear term is smaller, it does increase as true energy increases in a nature anticipated of leakage.

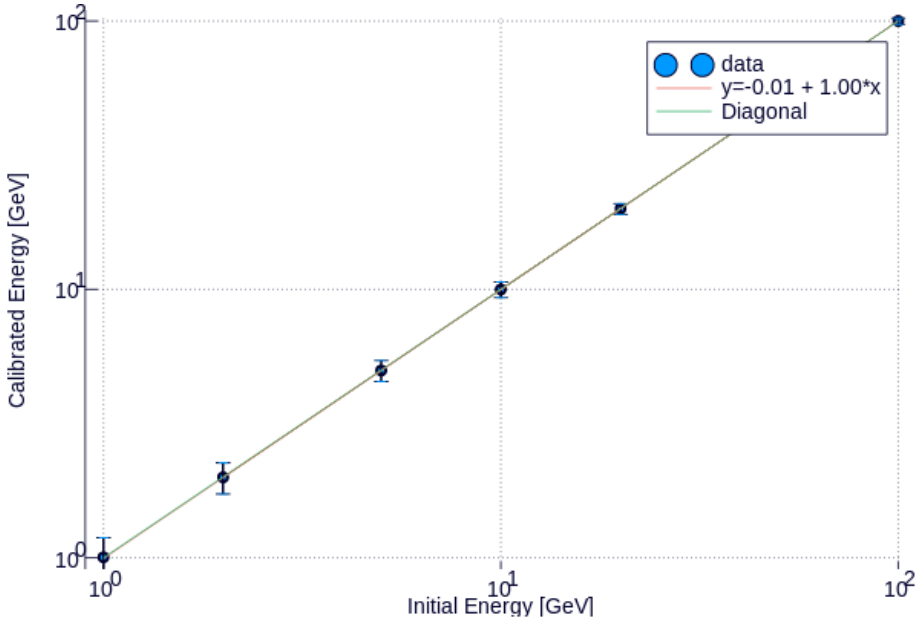

FIG. 14: The best linear fit when comparing the expected, true shower energy with the nonlinearly calibrated, reconstructed energy with calibration constants from Eqn. 5. The best fit line of $y = 1.00x - 0.01$ is closer to the ideal case of $y = x$ than the linear fit equation $y = 0.99x + 0.06$.

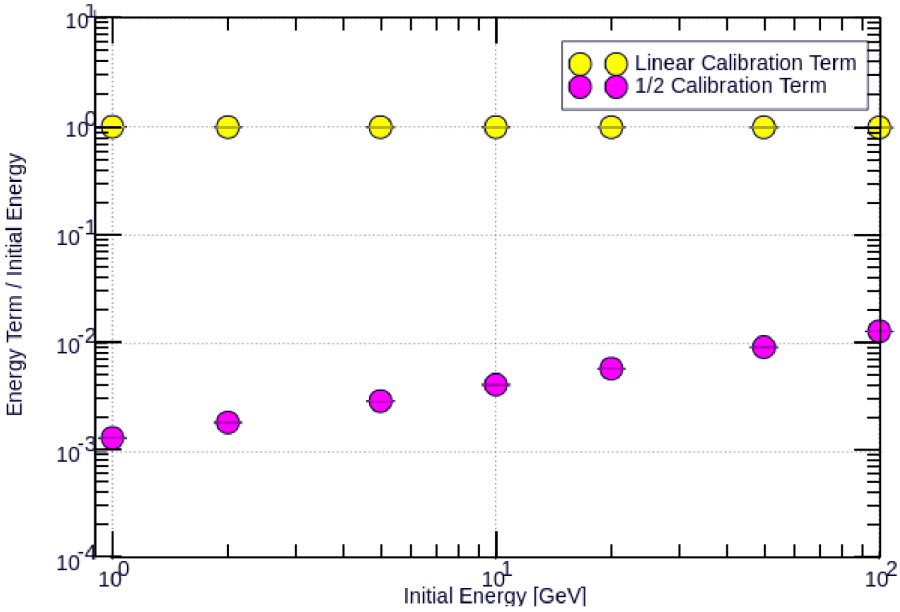

FIG. 15: The contribution of linear and nonlinear ("1/2") calibration terms to overall calibration. As expected, the nonlinear (pink) term contributes far less to the overall calibration than the linear (yellow) term, but its contribution increases as a function of true particle energy. This characteristic is to be expected of leakage, which the nonlinear term is intended to account for.

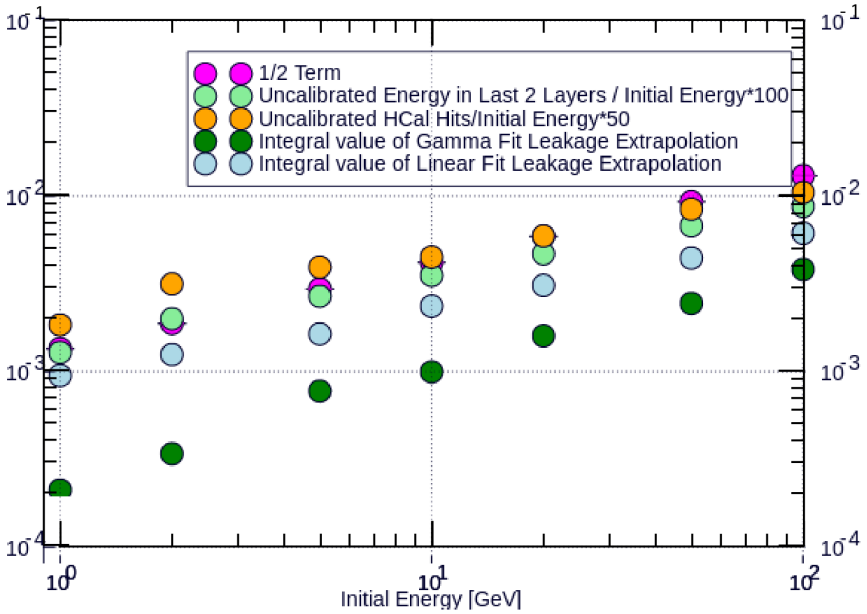

FIG. 16: The contribution of the nonlinear ("1/2") calibration term compared to four leakage estimation methods from Section IV. The nonlinear term, by design, follows the same trend as the leakage estimation methods indicating that the term is appropriately estimating leakage and incorporating the information into the overall calibration.

To further confirm that the nonlinear term is really accounting for leakage directly, the contribution of the nonlinear ("1/2") term to calibration is compared to other leakage prediction methods explored in Section IV. Figure 16 shows the nonlinear contribution (pink) compared to other leakage estimation methods. Figure 17 shows the same data

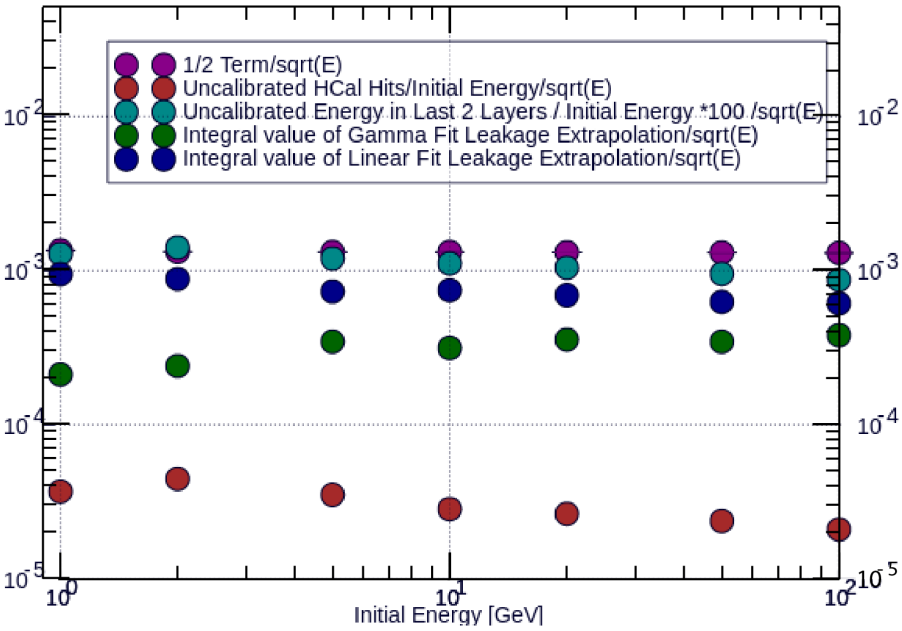

FIG. 17: The contribution of the nonlinear ("1/2") calibration term scaled by $1/\sqrt{E_{true}}$ compared to four leakage estimation methods from Section IV, identically scaled. The nonlinear term, by design, follows the same trend as the leakage estimation methods indicating that the term is appropriately estimating leakage and incorporating the information into the overall calibration.

scaled by $1/\sqrt{E_{true}}$, where the nonlinear term data points have a slope of zero. In both cases, the nonlinear term closely follows the behavior of all leakage estimation methods, indicating that the $n = 1/2$ choice was appropriate to incorporate leakage approximation into electromagnetic shower calibration.

In addition to approaching a better overall calibration from Fig. 15, the ratio of calibrated shower energy to true particle energy (originally in Fig. 5) improves in high energy regions of the plot (Fig. 18). This is due to the nonlinear term incorporating the effect of leakage into the calibration.

One concern is whether calibration has a negative effect on the energy resolution, with calibration uncertainties exceeding those of the energy resolution. Error in calibration per energy resolution R,

$$\left(1 - \frac{E_{calibrated}}{E_{true}}\right) R \;=\; \left(1 - \frac{E_{calibrated}}{E_{true}}\right) \frac{\sigma}{\mu} \,, \tag{6}$$

shown in Fig. 19, indicates that overall the errors are well controlled and fall under 3% for showers of all energies. This is actually an improvement from the linear calibration case of Section III where uncertainties climb with true energy into high regions (Fig. 20).

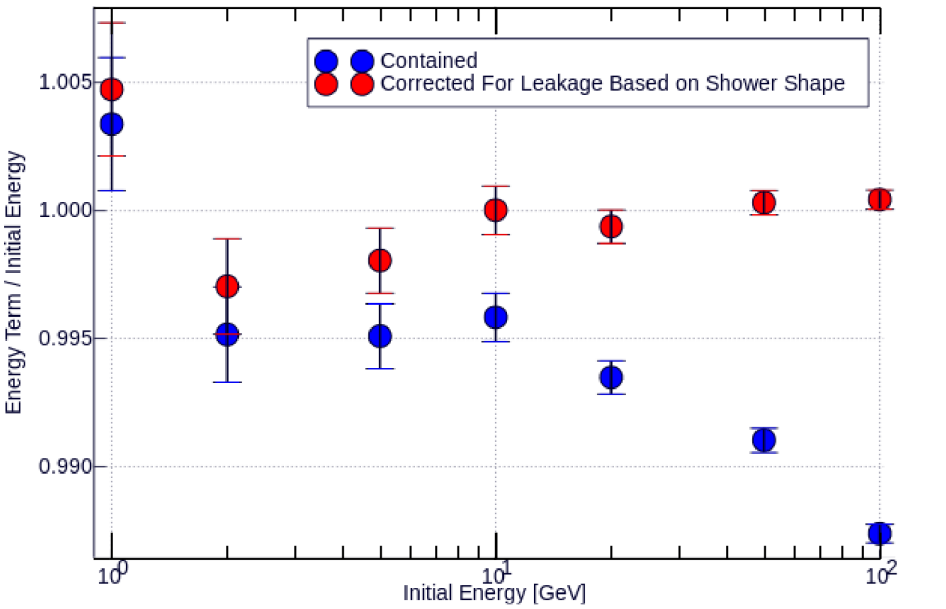

FIG. 18: The ratio of mean nonlinearly calibrated energy to its expected value for deposits contained within the ECal. For perfect calibration, this value should approach unity for every true energy. The decrease in the blue "contained" curve (from a linear calibration) at high energies is eliminated in the red curve which incorporates the nonlinear calibration, indicating that the nonlinear term is accounting for leakage at higher energies and improving the overall calibration.

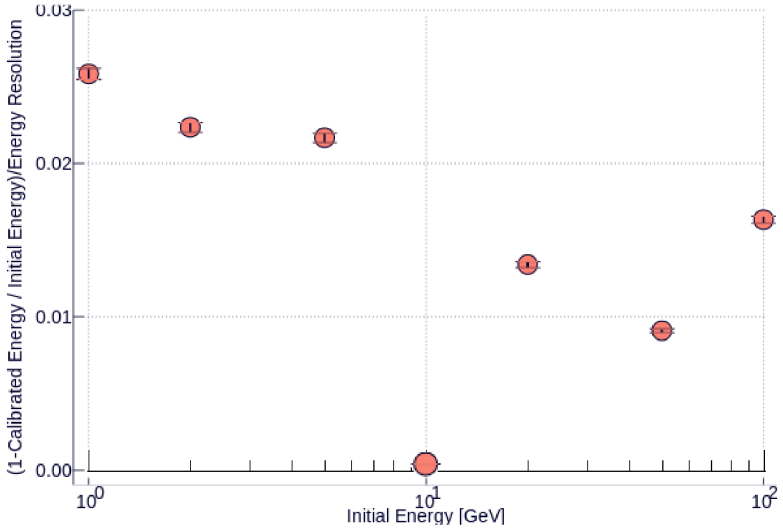

FIG. 19: The uncertainty in calibration per energy resolution (Eqn. 6) for full, nonlinear calibration. The overall errors are well controlled and contained within 3%.

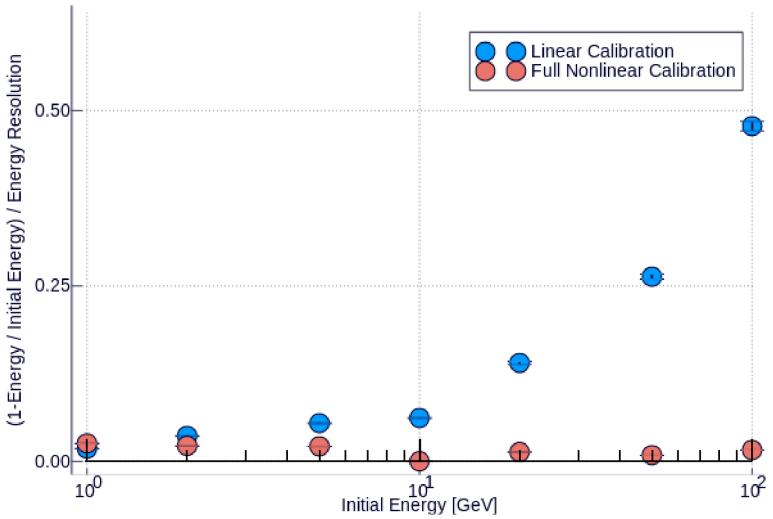

FIG. 20: The uncertainty in calibration per energy resolution (Eqn. 6) for full, nonlinear calibration in pink and linear calibration in blue. The linear calibration technique does not control errors like the nonlinear case, especially at high energies where the uncertainty value increases exponentially.

VI. CONCLUSION AND FUTURE WORK

The SiD ECal is a robust calorimeter, and is necessary for the success of SiD. Its geometry incorporates factors into its calibration due both to the overlapping module structure and to its finite depth that cannot fully contain electromagnetic showers from high energy particles. The energy lost into the HCal, or leakage, is both energy- and angle-dependent. The energy-dependent nature of this leakage can be incorporated into ECal calibration by including a nonlinear "1/2" calibration term that compensates for anticipated leakage and factors that value back in. This procedure increases the accuracy of calibration while controlling overall errors and allowing for the ECal's small energy resolution to remain a larger source of error than that from calibration itself.

These studies can be improved and built upon in many ways, such as incorporating the nonlinear calibration factor from these studies into the more robust SiD reconstruction and digitization framework and investigating the effect of the angle φ on leakage and therefore its effect on calibration. Studies such as these involving SiD calorimeter calibration and optimization are ongoing at the University of Oregon.

VII. ACKNOWLEDGMENTS

We would like to thank and acknowledge the SiD Optimization group for providing technical support and constructive feedback during the entire duration of these studies.

[1] T. Behnke, J. Brau *et al.*, "The Interntional Linear Collider Technical Design Report - Volume 4: Detectors," `arXiv:1306.6329v1[physics.ins-det]`
[2] `https://github.com/jstrube/CalorimeterCalibration`
[3] E. Longo and I. Sestili, Nucl. Instrum. Meth. 128, 283, (1975).
[4] G. Grindhammer and S. Peters, "The Parameterized Simulation of Electromagnetic Showers in Homogeneous and Sampling Calorimeters," `arXiv:hep-ex/0001020`